JOURNAL OF MATERIALS SCIENCE **35** (2000) 3069–3075

Dendrite morphologies of the metastable phase from undercooled Fe-30at% Co melts and its stabilities

LI MINGJUN*, YANG GENCANG, ZHOU YAOHE
State Key Laboratory of Solidification Processing, Northwestern Polytechnical University, Xi'an, 710072, People's Republic of China
E-mail: mingjun@mpie.de

Five typical dendrite morphologies of the metastable bcc phase from undercooled Fe-30 at % Co melts have been observed by TEM technique. The morphologies of the metastable phase exhibited well-developed dendrite with the primary trunk and second arms, well-developed second arms, radiated structure, lath structure, and bifurcated structure. The crystal growth mode and the formation of different dendrite morphologies were discussed on the basis of the morphological patterns from undercooled melts. In the mean while, the breakage mode for the primary dendrite was suggested according to the observation of microstructures of the alloy solidified at various undercoolings. The EDS (Energy Dispersive Spectrum) analysis has confirmed enrichment of the solute Co in metastable dendrite cores in comparison to that predicted from the view of equilibrium solidification. Further investigation after annealing showed that the solute diffusion controlled the stability of the metastable phase; the disappearance of dendrite morphologies was mainly attributed to the constituent homogenization within dendrite cores and the decrease in the number of dendrite cores was chiefly owing to the solute diffusion between dendrite cores and the subsequently solidified equilibrium phase.

1. Introduction

Solidification of undercooled melts can produce considerable novel phenomena not observed in usual castings, including refined microstructure [1, 2], solute trapping [3], reduced constitutional segregation [4], transition of morphological aspects [5], metastable phases [6], *et al*. Since the pioneering work of Cech [7] who observed the crystalline metastable bcc phase from the undercooled Fe-Ni alloy in a drop-tube experiment, much work has been carried out to investigate the formation of metastable phases from undercooled hyperperitectic systems. Based on the double recalescence profile in the solidification of the undercooled $Fe_{90}Ni_{10}$ alloy [8], Herlach and co-workers concluded that the metastable bcc phase was produced during the first recalescence and the solidification of the equilibrium fcc phase led to the second recalescence behavior. They also found that the formation of the metastable phase in the system is favorable during competitive nucleation of bcc and fcc phases when the undercooling is larger than a certain critical undercooling. Unfortunately, no traces of the metastable bcc phase can be observed over the complete concentration range in their study [9]. Another interesting system exhibiting competitive nucleation is the Fe-Cr-Ni alloy. Koseki and Flemings [10–12] investigated the alloys systematically from the view of the thermal behavior [10], microstructure evolution [11] and phase selection [12], where they found dispersed particles embraced in some grains. They believed these particles were the metastable phase and nucleated primarily from the melts. However, they did not make any further investigation about the morphologies of these particles. Quasicrystals with five fold rotational symmetry which is incompatible with the translational symmetry of normal crystal phases, has attracted much interest since the pioneering wok by Shechtman *et al.* [13]. The bright field images reveal that the morphologies of the quasicrystalline phase exhibit rosette-like structure [14]. The selected-area diffraction patterns with five-fold symmetry of quasicrystalline phases in undercooled Al-Mn [15], Al-Co [16] and Al-Cu-Fe, Al-Cu-Co [17] alloys throw light on the formation of quasicrystal phases during recalescence, which is mainly limited to the competitive nucleation between the crystal phase and the quasicrystal phase.

This paper deals with dendrite morphologies of the metastable bcc phase from undercooled Fe-30 at % Co melts when the alloy is undercooled greater than the

* Author to whom all correspondence should be addressed. Present address: Department of Metallurgy, Max-Planck-Institute fuer Eisenforschung, Max-Planck-str.1, D-40237, Duesseldorf, Germany, Fax: +49, 211, 6792390.

critical undercooling $\Delta T = 204$ K for the formation of the metastable phase in the alloy. The EDS technique is utilized to reveal the composition difference of the metastable phase directly crystallizing from the melt. The stability of metastable dendrite cores has also been investigated after the identical specimen is annealed at 1473 K and 1673 K for different periods.

2. Experimental procedure

High purity elements of iron (Fe) and cobalt (Co) better than 99.8 wt. % are alloyed *in situ* with an approximate weight 5 g for each sample. Prior to melting, surfaces of metals are cleaned mechanically by grinding off the oxide layers and cleaned chemically by etching in HCl solution diluted by alcohol. The glass slag B_2O_3 is melted with the help of a graphite heater in a high frequency r.f. apparatus. The bulk metals with the composition of Fe-30 at. % Co are immersed immediately into the bottom of the quartz tubes and then melted with the protection of the glass slag. Several heating and cooling cycles are necessary to homogenize the melts. The nucleation of the melt is triggered with a glass rod at well-defined undercoolings at the upper surface of the sample since it has no effect on the nucleation of primary phase [18]. It is clear that no chemical reactions can occur between the melt and the glass slag, so the composition of the as-solidified specimens is equal to that of the original chemical constitution. The thermal behavior of samples is monitored by an infra pyrometer with an absolute accuracy, relative accuracy, and response time of less than 10 K, 3 K, and 5 ms, respectively. The cooling curve is calibrated with a standard $PtRh_{30}$-$PtRh_6$ thermal couple, which is encapsulated in a silica tube and then immersed into the melt in the identical condition to verify the melting point and undercoolings of the alloy. Further detailed experimental procedure has been described elsewhere [19].

The sample is cut and then polished for optical observing the microstructures and then thinned for identifying the morphological aspects. The transmission electron microscope (JEM-200cx) technique is utilized to analyze morphologies of the metastable bcc phase crystallizing from highly undercooled Fe-30 at % Co alloys. The EDS is applied to detect the chemical composition difference of the primary phase and the subsequently solidified product.

The sample of Fe-30 at % Co alloy obtained at the maximum undercooling is cut into several pieces for annealing at 1473 K and 1673 K for various periods so as to reveal stabilities of the metastable phase.

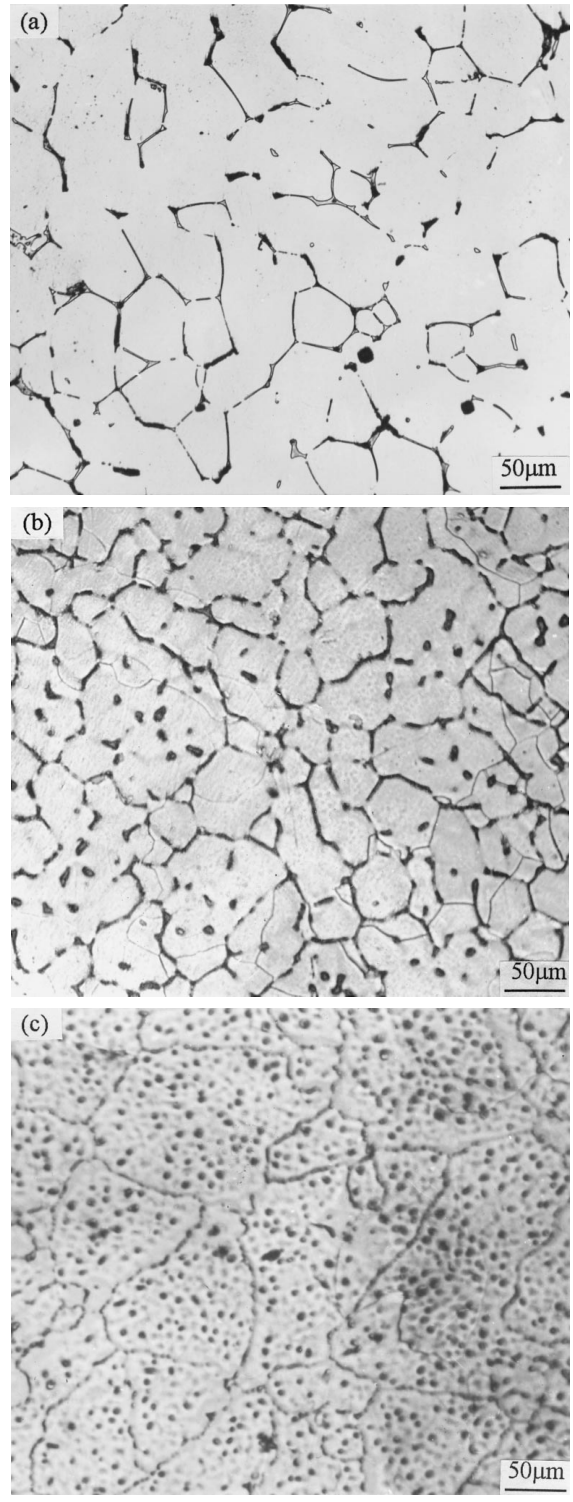

Figure 1 Microstructures of the Fe-30 at % Co alloy solidified at (a) $\Delta T = 58$ K, (b) $\Delta T = 204$ K and (c) the maximum undercooling $\Delta T = 308$ K.

3. Results

3.1. Dendrite morphologies of the metastable phase

The Fe-Co equilibrium phase diagram is similar to that of Fe-Ni system with a peritectic reaction at the Fe-rich part near the melting temperature. Based on the regular solution mode, the metastable extension has been calculated with the content of element Co larger than 16.9 at %, which makes it possible for the metastable bcc and the stable fcc phases to competitively nucleate when the melts are undercooled greater than the critical undercoolings for the formation of the metastable bcc phase. From the view of classical nucleation theory, the detailed competitive nucleation of both phases based on numerical calculation has been described elsewhere when the undercooling of Fe-30 at % Co melts is sufficiently large [20]. The metastable bcc phase is nucleated primarily from the melt when the undercooling is larger than critical undercooling $\Delta T = 204$ K by observing the microstructure. Fig. 1 shows three microstructures of the alloy solidified at $\Delta T = 58$ K

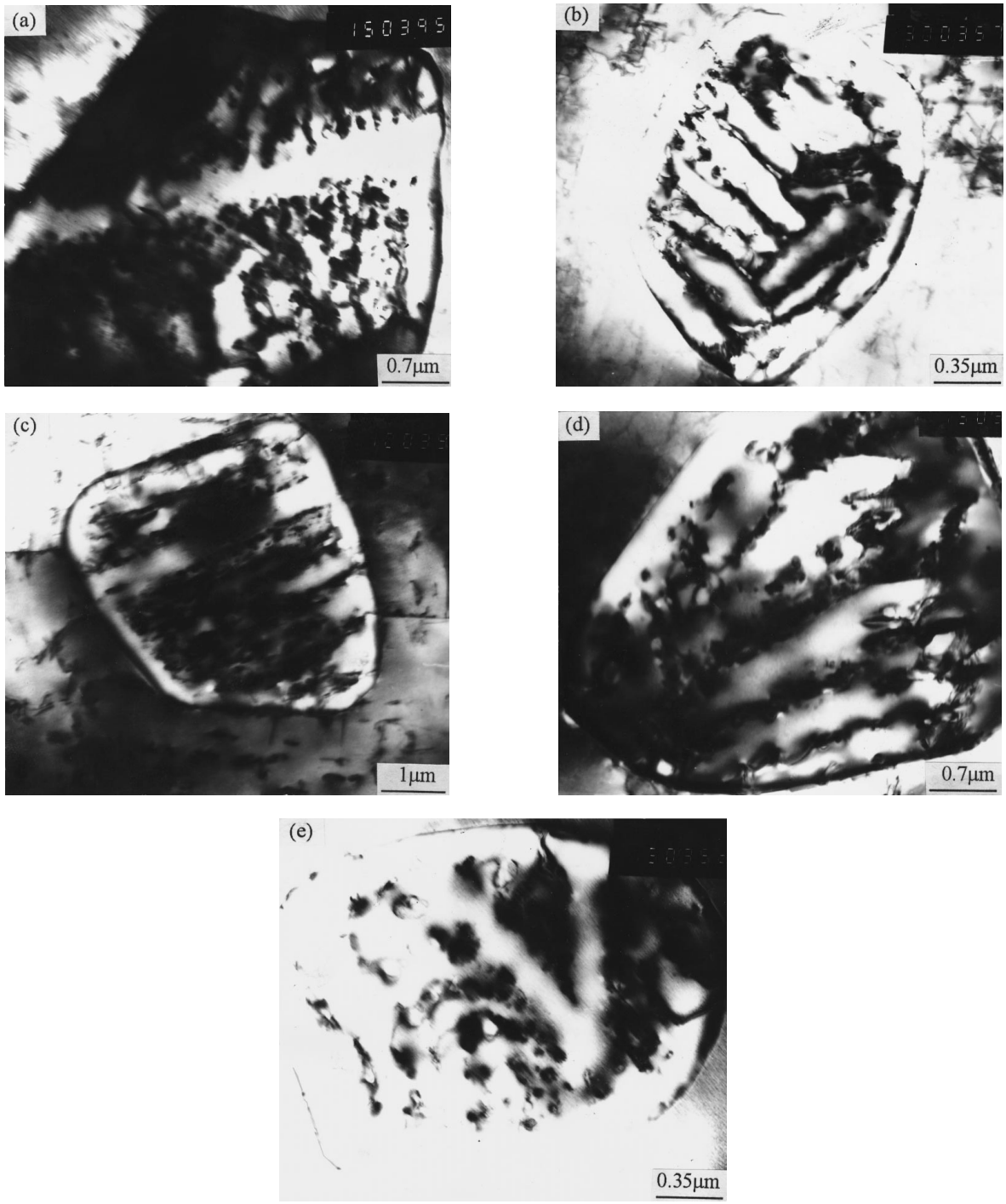

Figure 2 Five typical dendrite morphologies of the metastable bcc phase from Fe-30 at. % Co melts.

(Fig. 1a), critical undercooling for the formation of metastable bcc phase $\Delta T = 204$ K (Fig. 1b) and the maximum undercooling $\Delta T = 308$ K (Fig. 1c). The equiaxed grains display single-phase characteristic in Fig. 1a. However, one can see clearly that one or two particles are embedded in grains in Fig. 1b, whereas in Fig. 1c, many particles are embraced in grains. We term the particles "dendrite cores" as suggested by Koseki and Flemings [11], who found dispersed particles embedded in some grains in undercooled Fe-Cr-Ni alloys. We define the undercooling at which the alloy is solidified with one or two particles in one grain as the critical undercooling. It is interesting that the primary phase exhibits dispersed dendrite cores rather than dendrite skeleton. We will discuss the breakage pattern of the primary phase during rapid recalescence in the section below. Fig. 2 shows five typical dendrite morphologies of the metastable bcc phase from Fe-30 at % Co melts. Fig. 2a is the morphology with the well-developed primary trunk and the second arms, indicating that the dendrite core is produced directly from the melt rather than from the solid during solid phase transformation (at the given composition, the alloy may undergo a martensite phase transformation from γ to α at about 1250 K). Fig. 2b is another morphology with the well-developed second arms, in which the primary skeleton could not be discerned. Consider half of the second arms in Fig. 2b are remelted, the structure left is, of course, the lath structure as shown in Fig. 2c. Fig. 2d presents the radiated structure different from morphologies in Fig. 2a–c.

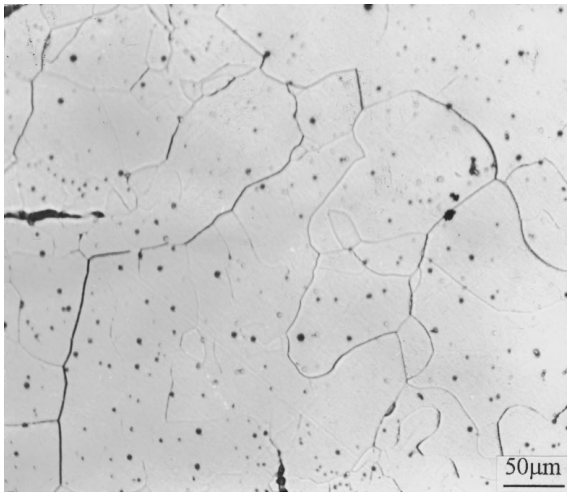

Figure 3 The microstructure of Fe-30 at % Co alloy solidified at the maximum undercooling after annealing at 1673 K for 10 min.

One can even see the nucleation site, from which the radiated branches may grow. Fig. 2e is the morphology of the alloy with only a bifurcated structure, in which the primary skeleton and the second arms can not be distinguished clearly.

3.2. The microstructures of the alloy after annealing

Since the bcc phase solidified beyond the critical undercooling is metastable, it is of specific importance to investigate the stability of the metastable phase for further application to the alloy. Fig. 3 presents the microstructure of the alloy solidified at $\Delta T = 308$ K after annealing at 1673 K for 10 min. In comparison with the microstructure prior to annealing in Fig. 1c, the number of the dendrite cores is drastically reduced after annealing. Fig. 4 shows the bright-field images of dendrite cores after annealing. The dendrite morphologies have completely vanished in Fig. 4a, being only a bright circularity. In Fig. 4b, only a very small part in the dendrite-core center can be found after careful observation. There is a band between two dendrite cores in Fig. 4c, showing that the structure of the bright circularity is similar to that of linking band. The decrease of dendrite-core numbers and the disappearance of morphologies after annealing indicate clearly that the stability of dendrite cores in the alloy is limited to the solute diffusion rather than a sudden phase transition, unlike the martensite phase transformation in steel. Fig. 5 is the microstructure of the alloy solidified at $\Delta T = 308$ K after annealing at 1473 K for 1 h. We can see that the number of the dendrite cores is similar to that annealed at 1673 K for 10 min. Further analysis regarding to the morphologies of dendrite cores in this case shows similar results as that in Fig. 4.

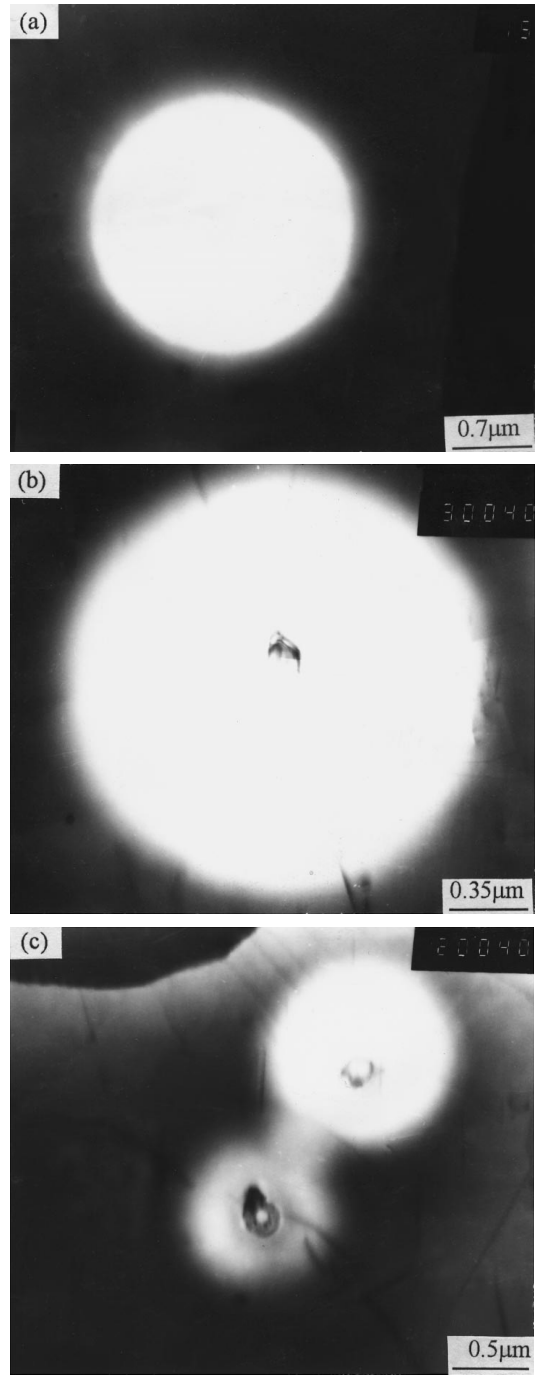

Figure 4 Bright-field images of dendrite cores after annealing (a) the dendrite morphologies have completely vanished, with only a bright circularity, (b) only a smaller part in the dendrite core is left, and (c) there is a link between two dendrite cores.

4. Discussion

4.1. Crystal growth mode of the metastable phase in undercooled melts

Based on the absolute stability theory of solid/liquid interface developed by Mullins and Sekerka [21], the solidification interface of an undercooled melt is always unstable due to the negative temperature gradient in front of the interface. Trivedi and Kurz [22] confirmed that a velocity greater than critical value V_{abs} could lead to the absolute stability of a planar interface without considering the crystallization heat conducted out through solids. However, it is impossible for general bulk alloy to solidify at such a high rate that V_{abs} denotes the upper limit of the solidification of the alloy when the ideal collision of atoms is taken into account. The critical value V_{abs} decreases significantly when considering the dissipation of crystallization heat through the solid during solidification [23]. This solidification behavior

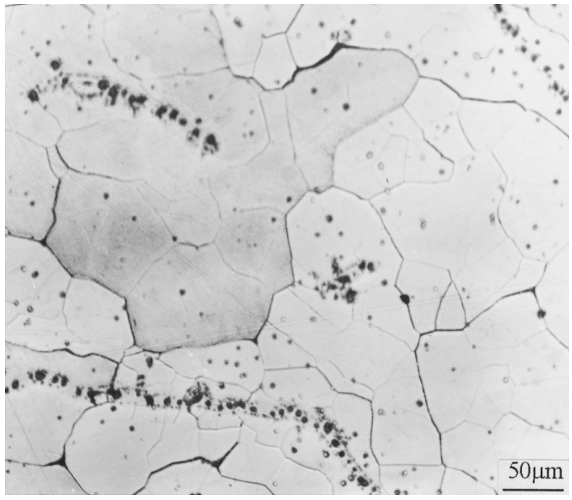

Figure 5 The microstructure of Fe-30 at % Co alloy solidified at the maximum undercooling after annealing at 1473 K for 1 h.

might be observed in atomization experiment since that the potential heat could dissipate rapidly. As a matter of fact, the recalescence interval in the solidification of a bulk sample is so short that only a little crystallization heat could be conducted out though the solid within several microseconds. Except Xuezhi Zhang [24], no one has observed a planar front in the undercooled bulk specimens. However, we have commented the paper from the view of the current dendrite growth theory [25]. We believe that the crystal growth mode in undercooled bulk melt is of dendrite pattern no matter what kind of phases, in the alloy fcc or bcc phase, is produced.

4.2. Dendritic growth and solute trapping of the metastable phase in undercooled Fe-30at%Co melts

Compared with dendrites in usual castings, the high undercooling might lead to a finer structure of the primary bcc phase, because the recalescence interval is so short that it is impossible for the primary metastable bcc phase to ripen completely. Theoretically, the dendritic tip radii can be calculated on the basis of the BCT model [26], which can be read as:

$$\Delta T = \Delta T_c + \Delta T_t + \Delta T_r + \Delta T_k \tag{1}$$

where ΔT_t is the thermal undercooling, ΔT_c the constitutional undercooling, ΔT_r the Gibbs-Thomson undercooling due to strong curvature at the tip of the dendrite and ΔT_k the kinetic undercooling of the interface. The expressions for ΔT_t, ΔT_c, ΔT_r, and ΔT_k have been described elsewhere in detail [27]. Equation 1 gives a relation between the undercooling ΔT and the product VR in terms of Peclet numbers. Taking into account the marginal stability criterion [26], the general theory of free dendritic growth yields a second equation for the radius R of the dendrite tip:

$$R = \frac{\Gamma/\sigma^*}{P_t \Delta T_{hyp}(1-n) - \dfrac{2P_c mc_0(1-k)}{1-(1-k)Iv(P_c)}(1+g)} \tag{2}$$

with

$$n = \frac{1}{\left(1+1/\left(\sigma^* P_c^2\right)\right)^{1/2}} \tag{2a}$$

$$g = \frac{2k}{1-2k-\left(1+1/\left(\sigma^* P_c^2\right)\right)^{1/2}} \tag{2b}$$

where P_c, P_t are respectively the thermal and solute Peclet numbers, I_v is the Ivantsov function, ΔT_{hyp} is the hypercooling of the alloy, Γ is the Gibbs-thomson coefficient, k is the effective partition coefficient and $\sigma^* = 1/4\pi^2$ is the stability constant. Equation 1 together with Equation 2 allows a unique calculation of the tip velocity V as a function of the melt undercooling ΔT.

Using the characteristic data for the sample system as given elsewhere [20], the crystal growth velocities as well as the dendrite tip radii with respect to the undercoolings has been calculated as shown in Fig. 6. Comparing the theoretical results of the dendrite tip radius with the experimental value (in Fig. 2a), we can tell that the size of primary trunk is much larger than that in numerical simulation. Schwarz *et al.* [28] developed a fragmentation mode for primary dendrite after incorporating the Rayleigh instability, in which the trunk radius $R(\Delta T)$ is correlated to the dendrite tip radius $R_{tip}(\Delta T)$, via a proportionality constant, $R(\Delta T)/R_{tip}(\Delta T) = 20$. Based on the theoretical tip radii of the dendrite formed during recalescence at undercoolings beyond 204 K, as shown in Fig. 6, the size of primary trunk radius can be available being 0.5–0.7 μm in scale when the proportionality is considered. Obviously, this result fits well with the experimental in magnitude. The arm spacing in the dendrite cores can also be evaluated, which is approximately in the same magnitude as the dendritic tip radii in rapid solidification.

The solute trapping due to rapid advancement of the liquid-solid interface also becomes severe according to an effective partition coefficient k_e suggested by Aziz [29] when undercooling are sufficiently large,

$$k_e = \frac{k_0 + V/V_D}{1 + V/V_D} \tag{3}$$

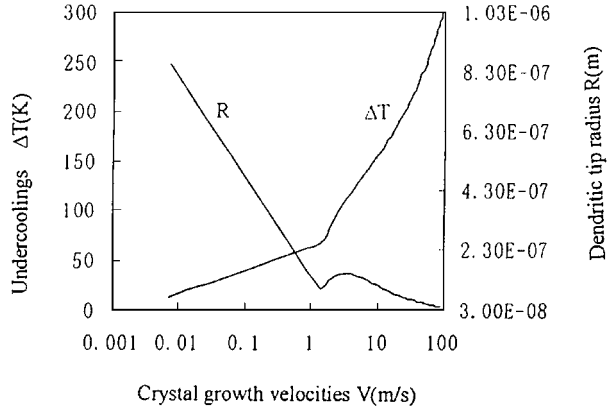

Figure 6 The calculated dendritic growth velocities and dendritic tip radius of the metastable bcc phase in undercooled Fe-30at% Co melt as a function of undercoolings.

where $V_D = D/a_0$ is the diffusion velocity of the solute, and k_0, D and a_0 are the equilibrium solute partition coefficient, the solute diffusivity, and the characteristic length of the solute diffusion in the liquid, respectively. Here, we can see that the higher the advancement of the solid-liquid interface, the more the solute will be trapped in the as-solidified product. The EDS (Energy Dispersive Spectrum) analysis has confirmed the enrichment of the solute Co in the metastable phase. The average content of element Co in above-mentioned dendrite cores is 28.65 at %, in comparison to the equilibrium solidification. This again proves that the dendrite cores are primarily formed during rapid recalescence rather than the precipitates.

4.3. The breakage mode of the primary dendrite

The solute trapping and the finer structure may vary the melting point of the primary phase significantly due to the solute redistribution and strong curvature effect of the finer dendrite. The temperature rise after rapid recalescence may be even higher than the melting point of the metastable phase. So the primary metastable bcc phase will be remelted into isolated dendrite cores at the solid-liquid interface and these dendrite cores disperse in remaining liquids. This breakage mode for the primary metastable phase is supported by the microstructure with dispersing dendrite cores. It is worth noting that the sizes of the dendrite cores in Fig. 2 are far from identical, i.e., some dendrite cores are several times larger than others. Since the sectioning position is somewhat random, we can assume the dendrite cores observed are sectioned through the diameter direction. Consequently, the size of dendrite cores can be comparable. The non-uniform remelting of the solids owing to the temperature fluctuation and the solute segregation in the alloy may lead to the formation of different sizes of dendrite cores. No matter what sizes of the dendrite cores are, they are more or less a part of dendrite structure.

As we can see, the metastable phase exhibits different dendrite morphologies even in one specimen. Here, we will discuss the formation of dendrite morphologies of the metastable phase. Fig. 7a schematically shows one primary dendrite of the bcc phase at the solid-liquid interface at the onset of its formation. It should be noted that the solidification of the dendrite is far from equilibrium, so the dendrite in this case may differ from that in near equilibrium castings. The sudden temperature rise due to recalescence may remelt the primary dendrite into several pieces. Since the remelting of the dendrite is somewhat random, various morphologies may be observed in the specimen. Here, we only focus on those dendrite cores, from which the dendrite morphologies of the primary integrated structure may be reflected more or less. Consider the primary dendrite has been remelted into several pieces as demonstrated in Fig. 7b. Part A, B, C, D, and E may form the dendrite cores with similar morphologies as shown in Fig. 2a–e, respectively. Of course, the morphologies in Fig. 2 may be observed from different primary dendrites in stead from one primary dendrite.

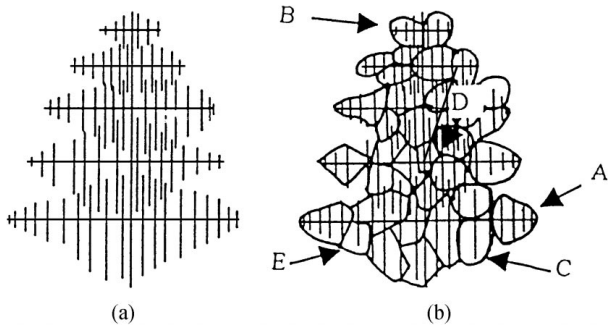

Figure 7 Schematic diagram for the formation of different morphologies in undercooled melts. (a) primary dendrite at the onset of its formation and (b) the supposed remelting resulted in the various dendrite morphologies.

4.4. Stabilities of dendrite cores after annealing

As we have pointed out, the stability of the dendrite cores in the alloy is limited to the solute diffusion at high temperature. Consider that the solute diffusion between the dendrite cores and the subsequently solidified product is stable under the annealing condition, the stability of the dendrite cores can be accounted for citing the well-known Fick's first law:

$$J^i = -D^i \operatorname{grad} C^i \tag{4}$$

where J^i is the instantaneous net flux of species i, or diffusion current per unit area, and grad C^i is the gradient of the concentration C^i of i. It is reasonable to suppose that the gradient of the solute Co in dendrite cores in one specimen is approximately identical, so the constituent homogenization, namely, the stability of dendrite cores is primarily limited to the diffusion coefficient D, which usually is temperature dependent with two constants D_0 and Q occurring in the Arrhenius equation:

$$D = D_0 \exp\left(-\frac{Q}{RT}\right) \tag{5}$$

where D_0 is pre-exponential factor, Q is the activation energy for diffusion; R and T are the gas constant and absolute temperature, respectively. Using characteristic data of D_0, Q from Ref. [30], we can calculate D at different temperatures of $T = 1473$ K, and $T = 1673$ K. The results indicate that the diffusion coefficient D_{1673} is about 9 times larger than D_{1473}. Although one specimen is annealed at 1673 K for only 10 min, larger diffusion coefficient D_{1673} makes the solute diffusion much faster than that at 1473 K and thus leading to the similar microstructures annealed at 1473 K for 1 h and 1673 K for 10 min, respectively. It is reasonable to predict that dendrite cores will disappear completely if the specimen is annealed at high temperature for long periods. It should be noted that sizes of dendrite cores are quite different as shown in Fig. 2. The smaller dendrite cores may disappear due to the constituent homogenization

during annealing, while the larger dendrite cores still exist in that the solute Co could not homogenize completely. The driving force for solute diffusion is the concentration gradient of the dendrite cores and equilibrium phase. The gradient near the circumference of dendrite cores is more much larger than elsewhere, whereas the center of the dendrite cores exhibits zero concentration gradient and thus the solute diffusion in the center is sluggish than that near circumference of dendrite cores. Consequently, the morphologies in center of certain dendrite cores are unchanged, as shown in Fig. 4b.

Another interesting characteristic is the shape of dendrite cores prior and posterior to annealing. The dendrite cores prior to annealing exhibit ellipsoid-like structures whereas those annealed show regular ball in three dimensions after comparing Figs 2 and 4. The solute within dendrite cores diffuses along the normal direction at the edge of interface between dendrite cores and the equilibrium phase, where the concentration gradient is much larger than elsewhere. Simply, the solute will enrich at the concave part around the dendrite cores and the solute at the convex part will diffuse more rapidly during annealing, and thus resulting in a regular and complete ball after annealing.

5. Conclusions

1. When the Fe-30at. %Co melt is undercooled greater than the critical undercooling for the formation of metastable bcc phase $\Delta T = 204$ K, bcc phase will primarily nucleate from the melt. The crystal growth mode of metastable bcc phase exhibits dendritic pattern even at the achievable maximum undercooling $\Delta T = 308$ K in present study. The primary dendrite of bcc phase is enriched the solute Co due to the rapid advancement of solid/liquid interface. The primary dendrite will break up as isolated dendrite cores dispersing in the remaining liquids. The morphologies of dendrite cores exhibit well-developed dendrite with primary trunk and second arms, well-developed second arms, radiated structure, lath structure, and bifurcated structure, respectively. These cores are more or less a part of the primary dendrite, so they exhibit accordingly various dendritic morphologies due to the random breakage of the primary dendrite. The classical BCT mode is applied to account for the size of the primary trunk and side branches, which fits well with the experimentally observed structure.

2. The stability of the dendrite cores is limited to the solute diffusion rather than the sudden phase transformation. The temperature and periods under which the sample is annealed play a significant role in determining the stabilities of dendrite cores. The disappearance of dendrite morphologies was mainly attributed to the constituent homogenization within dendrite cores and the decrease in the number of dendrite cores was chiefly owing to the solute diffusion between dendrite cores and the subsequently solidified equilibrium phase, since the solute element Co is enriched in dendrite cores during recalescence. The dendrite morphologies may vanish with only a bright circularity, in which the solute Co is more homogenous than that prior to annealing.

Acknowledgements

The authors express their appreciation to National Natural Science Foundation of China (Grant No. 5967 1045) for financial support.

References

1. G. D. MERZ and T. Z. KATTAMIS, *Metall. Trans. A.* **8A** (1977) 295.
2. T. Z. KATTAMIS, NASA CP-2337, 1984, 15.
3. M. G. CHU, Y. SHIOHARA and M. C. FLEMINGS, *Metall. Trans. A.* **15A** (1984) 1303.
4. T. Z. KATTAMIS and M. C. FLEMINGS, *Mod. Cast.* **67** (1967) 97.
5. Y. WU, T. J. PIOCCONE, Y. SHIOHARA and M. C. FLEMINGS: *Metall. Trans. A.* **18A** (1987) 915.
6. J. H. PEREPEZKO, *Mater. Sci. Eng.* **65** (1984) 125.
7. R. E. CECH, *Trans. AIME*. **206** (1956) 585.
8. D. M. HERLACH, *Mater. Sci. Eng*. **R12** (1994) 240.
9. R. WILLNECKER, D. M. HERLACH and B. FEUERBACHER, *Appl. Phys. Lett*. **49** (1986) 1339.
10. TOSHIHIKO KOSEKI and MERTON C. FLEMINGS, *Metall. Mater. Trans. A.* **26A** (1995) 2991.
11. *Idem., ibid*. **27A** (1996) 3226.
12. *Idem., ibid.* **28A** (1997) 2385.
13. D. SHECHTMAN, I. BLECH, D. GRATIAS and J. W. CAHN, *Phys. Rev. Lett.* **53** (1984) 1951.
14. X. Z. LI and K. H. KUO, *J. Mater. Res.* **8** (1993) 2499.
15. D. M. HERLACH, F. GILLESSEN, T. VOLKMANN, M. WOLLGARTEN and K. URBAN, *Phys. Rev. B.* **46** (1992) 5203.
16. J. SCHROERS, D. HOLLAND-MORITZ, D. M. HERLACH, B. GRUSHKO and K. URBAN, *Mater. Sci. Eng.* **A226–228** (1997) 990.
17. D. HOLLAND-MORITZ, D.M. HERLACH and K. URBAN, *Appl. Phys. Lett.* **71** (1993) 1196.
18. D. M. HERLACH, B. FEUERBACHER and E. SCHLEIP, *Mater. Sci. Eng.* **A133** (1991) 795.
19. LI MINGJUN, YANG GENCANG and ZHOU YAOHE, *Metall. Mater. Trans. A.* **30A** (1999) 2941.
20. LI MINGJUN, LIN XIN, SONG GUANGSHENG, YANG GENCANG and ZHOU YAOHE, *Mater. Sci. Eng.* **A268** (1999) 90.
21. W. W. MULLINS and R. F. SEKERKA, *J. Appl. Phys.* **35** (1964) 444.
22. R. TRIVEDI and W. KURZ, *Acta Metall.* **34** (1986) 1663.
23. A. LUDWIG, *Acta Metall. Mater.* **39** (1991) 2795.
24. XUEZHI ZHANG, *Mater. Sci. Eng*. **A247** (1998) 214.
25. LI MINGJUN, YANG GENCANG and ZHOU YAOHE, *ibid.* **A270** (1999) 267.
26. W. J. BOETTINGER, S. R. CORIELL and R. TRIVEDI, in "Rapid Solidification Processing: Principles and Technologies IV," edited by R. Mehrabian and P.A. Parrish (Claitor's, Baton Rouge, LA, 1988) p. 13.
27. M. SCHWARZ, A. KARMA, K. ECKLER and D. M. HERLACH, *Phys. Rev. Lett.* **73** (1994) 1380.
28. LI MINGJUN, YUE YUFANG, SONG GUANGSHANG, YANG GENCANG and ZHOU YAOHE, *Acta Metall. Sinica*. **35** (1999) 517.
29. M. J. AZIZ, *J. Appl. Phys*. **53** (1982) 1158.
30. E. A. BRANDES, "Smithells Metals Reference Book," 6th ed., (Landen, Butterworths & Co. Ltd., 1983) p. 13.

Received 19 February
and accepted 18 August 1999